The Astrophysical Journal, 927:46 (14pp), 2022 March 1 https://doi.org/10.3847/1538-4357/ac4474
© 2022. The Author(s). Published by the American Astronomical Society.
OPEN ACCESS

HCN and HCO^+ in Planetary Nebulae: The Next Level

D. R. Schmidt[1], K. R. Gold[2,3], A. Sinclair[4], S. Bergstrom[1], and L. M. Ziurys[3,5]
[1] Department of Physics and Astronomy, Franklin & Marshall College, PO Box 3003, Lancaster, PA 17604-3003, USA
[2] Bryn Mawr College, 101 North Merion Avenue, Bryn Mawr, PA 19010-2859, USA
[3] Department of Chemistry and Biochemistry, University of Arizona, PO Box 210041, Tucson, AZ 85721-0041, USA
[4] Department of Physics & Astronomy, Swarthmore College, 500 College Avenue, Swarthmore, PA 19081-1397, USA
[5] Department of Astronomy, Arizona Radio Observatory, and Steward Observatory, University of Arizona, 933 North Cherry Avenue, Tucson, AZ 85721-0065, USA
Received 2021 September 5; revised 2021 December 3; accepted 2021 December 13; published 2022 March 3

Abstract

Observations of HCN and HCO^+ have been carried out toward 13 planetary nebulae (PNe) using the facilities of the Arizona Radio Observatory (ARO). These nebulae represent a wide range of morphologies and ages (∼2000–28,000 yr). For both molecules, the $J = 1 \rightarrow 0$ transitions at 88–89 GHz and the $J = 3 \rightarrow 2$ lines at 265–267 GHz were measured, together with CO lines ($J = 1 \rightarrow 0$, $2 \rightarrow 1$, and $3 \rightarrow 2$, depending on the source), using the ARO 12 m and Submillimeter Telescopes. HCN and HCO^+ were detected with at least one transition in 10 nebulae: He 2-459, Hu 1-1, K3-52, K3-65, M1-8, M1-40, M1-59, M2-53, M4-17, and NGC 6445. HCO^+ was additionally identified via two transitions in Na 2. Some observed line profiles were complex, with multiple velocity components tracing varied outflows. From radiative transfer modeling, column densities were established for HCN and HCO^+: $N_{tot}(HCN) = 0.005–1.1 \times 10^{14}$ and $N_{tot}(HCO^+) = 0.008–9.5 \times 10^{13}$ cm^{-2}. Gas densities of $n(H_2) \sim 10^5–10^7$ cm^{-3} were also determined for all PNe. Fractional abundances with respect to H_2, calculated using CO as a proxy, are $f(HCN) \sim 0.2–1.5 \times 10^{-7}$ and $f(HCO^+) \sim 0.3–5.1 \times 10^{-8}$. The abundances of HCN and HCO^+ did not significantly vary with nebular age to 28,000 yr. Combined with previous observations, at least 30 PNe contain HCN and/or HCO^+, indicating that polyatomic molecules are common constituents of these objects. The data strongly support a scenario where dense ejecta from PNe seed the interstellar medium with molecular material.

Unified Astronomy Thesaurus concepts: Astrochemistry (75); Planetary nebulae (1249); Radio astronomy (1338); Molecular spectroscopy (2095); Interstellar molecules (849)

1. Introduction

Planetary nebulae (PNe) represent the final stage in the lives of low-mass stars (∼1–8 $M_\odot$). In the preceding asymptotic giant branch (AGB) phase, copious mass loss (up to $10^{-4}\,M_\odot\,yr^{-1}$) strips the outer layers from the star, which flow away from the remnant carbon–oxygen core. Once the surface temperature of the central star has reached 30,000 K, its UV flux is capable of ionizing the ejected envelope and causing it to fluoresce, initiating the PN phase.

While the molecular composition of AGB stars has been extensively investigated, studies of the molecular content of PNe were quite limited until recently. This dearth of molecular observations was a result of current astrochemical theory, which speculated that the UV radiation from the emerging white dwarf star would photodissociate most molecules (e.g., Redman et al. 2003). Therefore, large-scale surveys of PNe were conducted of CO and H_2 but little else (e.g., Huggins & Healy 1989; Huggins et al. 1996, 2005; Hora et al. 1999; Sterling & Dinerstein 2008). A few sources were probed for more than diatomic species, including the very old Helix Nebula, NGC 7293 (Bachiller et al. 1997; Tenenbaum et al. 2009), and the very young PN NGC 7027 (Zhang et al. 2008). These observations suggested a paradigm change in understanding the chemistry of PNe, as HCN, HNC, HCO^+, H_2CO, c-C_3H_2, CCH, and CN were detected at one position in the Helix and CN, CCH, c-C_3H_2, HCN, HCO^+, HCS^+, HC_3N, and N_2H^+ in NGC 7027.

Over the past decade, further observations have clearly demonstrated that at least some PNe have a far richer chemical composition than ever speculated by theory. New studies have shown that polyatomic molecules are present throughout the Helix Nebula, including HCO^+, CCH, c-C_3H_2, and HCN (Zack & Ziurys 2013; Zeigler et al. 2013; Schmidt & Ziurys 2017a; Schmidt et al. 2018a). Further, Edwards & Ziurys (2013) and Edwards et al. (2014) reported the identification of numerous species toward the young PN NGC 6537, such as CN, HCN, HNC, CCH, CS, SO, H_2CO, HCO^+, and N_2H^+. The middle-aged nebula M2-48 also proved to be molecule-rich, with a similarly extensive chemical inventory of HCN, HNC, SiO, CS, SO, SO_2, HCO^+, and N_2H^+ (Edwards & Ziurys 2014; Edwards et al. 2014). Edwards et al. (2014) showed that the abundances of CS and HCO^+ did not appear to vary significantly with nebular age in five PNe spanning the range ∼900–10,000 yr.

Perhaps the most definitive work on the molecular composition of PNe is by Schmidt & Ziurys (2016, 2017a, 2017b). Schmidt & Ziurys (2016) reported the identification of HCN and HCO^+ in 13 of 17 target PNe in which CO had previously been detected. The nebulae comprised a diverse sample, with a variety of morphologies (elliptical, bipolar, quadrupolar) and ages, which were scattered relatively evenly across a range of 830–13,000 yr. Searches for HNC and CCH in the 11 nebulae in which HCN had been detected were also fruitful, yielding detection rates of 100% and ∼82%, respectively (Schmidt & Ziurys 2017a, 2017b). With this expanded data set in hand,

Original content from this work may be used under the terms of the Creative Commons Attribution 4.0 licence. Any further distribution of this work must maintain attribution to the author(s) and the title of the work, journal citation and DOI.

Table 1
Line Frequencies and Telescope Parameters

Transition	Telescope	Frequency (GHz)	Θ_b (arcsec)	η_B
HCN: $J = 1 \rightarrow 0$	12 m	88.6316	71	0.92
HCN: $J = 3 \rightarrow 2$	SMT	265.8864	28	0.71
HCO^+ $J = 1 \rightarrow 0$	12 m	89.1885	70	0.92
HCO^+ $J = 3 \rightarrow 2$	SMT	267.5576	28	0.71
CO: $J = 1 \rightarrow 0$	12 m	115.2712	54	0.9
CO: $J = 2 \rightarrow 1$	SMT	230.5380	32	0.73
CO: $J = 3 \rightarrow 2$	SMT	345.7959	21	0.55

Schmidt & Ziurys found, as suggested by Edwards et al. (2014), that molecular abundances did not notably vary with nebular age, in contrast to the predictions of chemical models. For example, Redman et al. (2003), who predicted the abundances of various species, including HCN, CCH, and HNC, calculated that they should be significantly depleted within the first ~1000 yr of the PN stage due to increased UV flux. The failure of the models has been attributed to insufficient shielding in the molecular clumps.

The molecular inventory has continued to expand for PNe. Observations have shown that the young planetary K4-47 is the most chemically complex to date, containing even larger polyatomic species like CH_3CN, H_2CNH, and CH_3CCH, none of which had been previously observed in PNe (Schmidt & Ziurys 2019). Further, observations of numerous ^{13}C-, ^{15}N-, and ^{17}O-bearing species have uncovered significant enhancements of these rare isotopes (Schmidt et al. 2018b; Schmidt & Ziurys 2019; Ziurys et al. 2020). Bublitz et al. (2019) reported the presence of polyatomic molecules HCN and HNC in NGC 6445 and NGC 6853, as well as HCO^+ in BD+30°3639. New molecular detections were also recently reported in NGC 7027, namely HeH^+ and CH^+ (Neufeld et al. 2020). Additionally, it should be noted that the most complicated molecules observed to date in the interstellar medium (ISM), C_{60} and C_{70}, are also constituents of PNe such as M1-12 and M1-20 (e.g., Cami et al. 2010; García-Hernández et al. 2010, 2011, 2012; Otsuka et al. 2013).

Such observations have yielded valuable insight into stellar evolution, chemical processing between the AGB and PN phases, and the role that PNe play in the cosmic recycling of molecular material. Although polyatomic molecules have now been identified in more than 20 PNe, there are thousands of these objects in the Galaxy (Parker et al. 2017). A major question therefore arises: are polyatomic molecules common to the majority of PNe? To further examine this question, we have conducted a search for HCN and HCO^+ in an additional 13 PNe through observations of their $J = 1 \rightarrow 0$ and $J = 3 \rightarrow 2$ rotational transitions. This new sample represents an age range of 2000–28,000 yr and morphologies from elliptical to multipolar. We detected these two molecules in most objects. Here we present our results and analysis and their implications for the molecular evolution of PNe.

2. Observations

The measurements were carried out using the facilities of the Arizona Radio Observatory (ARO) between 2019 February and 2021 March. HCN and HCO^+ were observed along with CO; line frequencies, beam sizes, and beam efficiencies are given in Table 1. Beam sizes ranged from 22″ to 71″; therefore, none of the PNe were likely resolved in these molecules, as is acceptable for a detection experiment. Note that the $J = 3 \rightarrow 2$ line of CO was observed for sources where the lower transitions suffered Galactic contamination.

The 3 mm ($J = 1 \rightarrow 0$) transitions of these molecules were conducted with the 12 m Atacama Large Millimeter/submillimeter Array (ALMA) prototype antenna on Kitt Peak, Arizona. A dual-polarization receiver with ALMA Band 3 sideband-separating (SBS) mixers was employed for these measurements, with typical image rejections >20 dB, intrinsic in the mixer architecture. Observations were conducted in the lower sideband in the case of HCN and HCO^+ and in the upper sideband (USB) for CO. The temperature scale T_A^* was determined by the chopper-wheel method, where $T_R = T_A^*/\eta_b$ and η_b is the main beam efficiency. The back end used was the ARO Wideband Spectrometer configured with 2×4 GHz of bandwidth for each receiver channel and 625 kHz spectral resolution (3.2–4.4 km s^{-1} for the frequencies in question). The 1 and 0.8 mm measurements ($J = 2 \rightarrow 1$ and $J = 3 \rightarrow 2$ lines; see Table 1) were conducted with the Submillimeter Telescope (SMT) on Mount Graham, Arizona. Dual-polarization receivers were used at 1 and 0.8 mm, consisting of ALMA Band 6 SBS mixers and double sideband SIS mixers. Image rejections of >15 dB are typical for the 1.3 mm receiver, and observations were conducted in the USB. The temperature scale for the SMT is T_A^*, as defined above. A 2048-channel filter bank with 1 MHz resolution (0.9–1.3 km s^{-1}) was employed as the primary back end for all observations, configured in parallel mode.

The list of sources is given in Table 2. Observations were typically conducted in beam-switching mode, with a throw of ±2′. Position-switching mode was used for NGC 6445, with an offset of 5′ in azimuth. Local oscillator shifts of 10 MHz were performed to check for image contamination. Pointing and focus were regularly checked using close-by strong continuum sources, ideally planets like Mars and Jupiter.

The targets for this search were culled from the large-scale CO surveys of Huggins & Healy (1989) and Huggins et al. (1996, 2005), as per Schmidt & Ziurys (2016). The main criteria were that the CO $J = 2 \rightarrow 1$ line had been detected and that there was no previously known HCN and HCO^+ emission. The exception here is NGC 6445, in which HCN and HCO^+ detections were first reported by Bublitz et al. (2019). The 13 nebulae selected for this work had the next strongest CO $J = 2 \rightarrow 1$ lines after those of Schmidt & Ziurys (2016), for which the minimum peak intensity was 50 mK.

3. Results

HCN and HCO^+ were detected in the majority of the 13 PNe selected for this study. The detection rates for these two molecules were 77% and 85%, respectively, and 77% for both species simultaneously. The observed spectra, as well as an optical and/or radio continuum image of the individual PNe, are shown in Figures 1–6. As the figures show, both HCO^+ and HCN were detected in He 2-459, Hu 1-1, K3-52, K3-65, M1-40, M1-59, M1-8, M2-53, M4-17, and NGC 6445. In addition, HCO^+ was also observed in Na 2. Some of the spectra display multiple velocity components, for example, M2-53. Others exhibit asymmetric profiles (e.g., Hu 1-1). Discussion of the individual sources is given below.

The spectra were fit with Gaussian profiles to establish line parameters, with a few exceptions, as noted below. Multiple velocity components were modeled when appropriate. These results are summarized in Table 3, which lists the peak

Table 2
Source Parameters

Source	R.A. (h m s) J2000.0	Decl. (deg arcmin arcsec) J2000.0	θ_s (arcsec)	Distance (kpc)	Age[a] (yr)	Morphology	C/O Ratio	Star Temperature (K)
He 2-459	20:13:57.9	+29:33:55.9	2[b]	7.2	2900	Bipolar	⋯	77,000
Hu 1-1	00:28:15.4	+55:57:54.5	10	3.9	6100, 6500[c]	Elliptical	2.1–2.5	114,000
K3-52	20:03:11.4	+30:32:34.1	2[b]	9.4	11,200	Bipolar/ irregular (?)	⋯	⋯
K3-65	04:15:54.5	+48:49:40.1	5	10.5	7300	⋯	⋯	⋯
K3-92	02:03:41.2	+64:57:37.9	13	7.1	12,500, 41,100[c]	Elliptical (?)	1.8	115,000
M1-8	06:53:33.8	+03:08:27.0	18	3.1	3400, 16,100[c]	Bipolar	2.5	161,000
M1-40	18:08:26.0	-22:16:52.9	10	2.8	1776,[c] 2600	?	⋯	88,000
M1-59	18:43:20.2	-09:04:49.1	5	3.5	4050,[c] 4700	Bipolar/ multipolar	⋯	117,490
M1-63	18:51:31.0	-13:10:36.6	4	7.3	3800	Elliptical/ bipolar (?)	⋯	115,100
M2-53	22:32:17.7	+56:10:26.1	18	3.6	6000	Elliptical	4.7	142,000
M4-17	20:09:01.9	+43:43:43.5	24	2.2	7200	Bipolar	⋯	⋯
Na 2	19:18:19.5	-11:06:16.2	25	9.0	28,400	Bipolar	⋯	⋯
NGC 6445	17:49:15.2	-20:00:34.5	33	1.4	3300,[c] 4700	Bipolar/ multipolar	∼1	184,000

Notes.
[a] Age derived in this work (see text).
[b] Angular size from this work (see text).
[c] Literature value.

intensities (T_A^*(K)), LSR velocities (V_{LSR}), and FWHM ($\Delta V_{1/2}$) for each detected line. As shown in the table, the intensities typically fall in the range ∼1–221 mK, and the line widths vary from 5 to 52 km s^{-1}. Representative fits to select spectra are given in Figure 7.

The small PN He 2-459 (with an estimated diameter of ∼1.″3) exhibits a bipolar morphology (Kwok & Aaquist 1993). We found that a source size of 2″ gave a good fit to our data, in reasonable agreement. A kinematic lifetime of ∼2900 yr was determined based on a distance of 7.24 kpc (Phillips & Márquez-Lugo 2011), an expansion velocity of 11.8 km s^{-1} (half the average CO line width), and a diameter of ∼2″. The central star is a Wolf-Rayet type of classification WC9 (Acker & Neiner 2003). While a C/O ratio is not available for He 2-459, it does exhibit a mix of carbon- and oxygen-rich dust features (Zhang & Kwok 1990). The $J = 3 \rightarrow 2$ transitions of HCN and HCO$^+$ were clearly detected in this source. H_2 was first detected in the nebula by Sterling & Dinerstein (2008). Huggins et al. (2005) noted the presence of Galactic contamination at 9 and 3 km s^{-1} in the $J = 2 \rightarrow 1$ line of CO, which is consistent with our observations of this transition and the $J = 3 \rightarrow 2$ spectrum.

Hu 1-1 is an elliptical PN with an angular size of ∼10″ (Phillips & Márquez-Lugo 2011). Stasińska et al. (1997) estimated an evolutionary age of 6500 yr. We calculate a kinematic age of 6100 yr using a revised distance of 3.86 kpc (Phillips & Márquez-Lugo 2011) and an expansion velocity of ∼15 km s^{-1}. The nebula is thought to be part of a binary system (Weidmann & Gamen 2011). According to studies of recombination lines, it is carbon-rich, with a C/O ratio of ∼2.1–2.5 (Delgado-Inglada & Rodríguez 2014; Peimbert et al. 2014). In this PN, the $J = 1 \rightarrow 0$ transitions of HCN and HCO$^+$ were detected (Figure 1). The $J = 3 \rightarrow 2$ transition was only identified in HCN. These spectra exhibit single-peaked, asymmetric profiles with a broad redshifted wing, as noted in CO by Huggins et al. (2005). Our $J = 2 \rightarrow 1$ line also clearly displays the broad redshifted wing.

The smallest nebula in our sample is K3-52, with a literature diameter of 0.″7 (Zhang & Kwok 1993). We found that a source size of 2″ resulted in a reasonable analysis, consistent with Zhang & Kwok (1993). No literature age is available for this PN, but given a distance of 9.42 kpc (Phillips & Márquez-Lugo 2011) and an expansion velocity of 4 km s^{-1} (half the CO line width), we have estimated a kinematic age of ∼11,170 yr. The $J = 1 \rightarrow 0$ and $J = 3 \rightarrow 2$ transitions of HCN and HCO$^+$ were detected in this source (Figure 2). A second, weak component is noticeable at ∼8 km s^{-1} in the HCN and HCO$^+$ $J = 3 \rightarrow 2$ spectra, though this feature is not readily apparent in other lines, mainly because it lies near Galactic contamination. The $J = 2 \rightarrow 1$ transition of CO was strongly affected by Galactic contamination, in agreement with what is seen in the $J = 3 \rightarrow 2$ line of CO and the $J = 1 \rightarrow 0$ line of HCN, with interstellar features present at ∼0.5 and ∼20.5 km s^{-1}.

With an angular size of 5″ (Aaquist & Kwok 1990), a distance of 10.512 kpc, and an expansion velocity of 17 km s^{-1}, a kinematic age of ∼7330 yr was estimated for the relatively unstudied source K3-65. Both HCN and HCO$^+$ were found in this nebula via their $J = 1 \rightarrow 0$ and $J = 3 \rightarrow 2$ lines (Figure 2). Huggins et al. (2005) noted that the CO $J = 2 \rightarrow 1$ line possessed a double-peaked profile with contamination at 29 km s^{-1}. A double-peaked profile is evident in our CO $J = 3 \rightarrow 2$ spectrum and possibly in HCN and HCO$^+$ but less apparent in the $J = 1 \rightarrow 0$ spectrum of the latter molecule.

Yet another source about which relatively little is known is K3-92. The nebula has an angular size of 13″ and is located at a distance of 7.11 kpc from Earth (Phillips & Márquez-Lugo 2011). Bohigas (2001) reported the morphology as elliptical based on optical and infrared images of the nebula, although Stasińska et al. (1997) listed the morphology as bipolar. Stasińska et al. (1997) derived an evolutionary age of

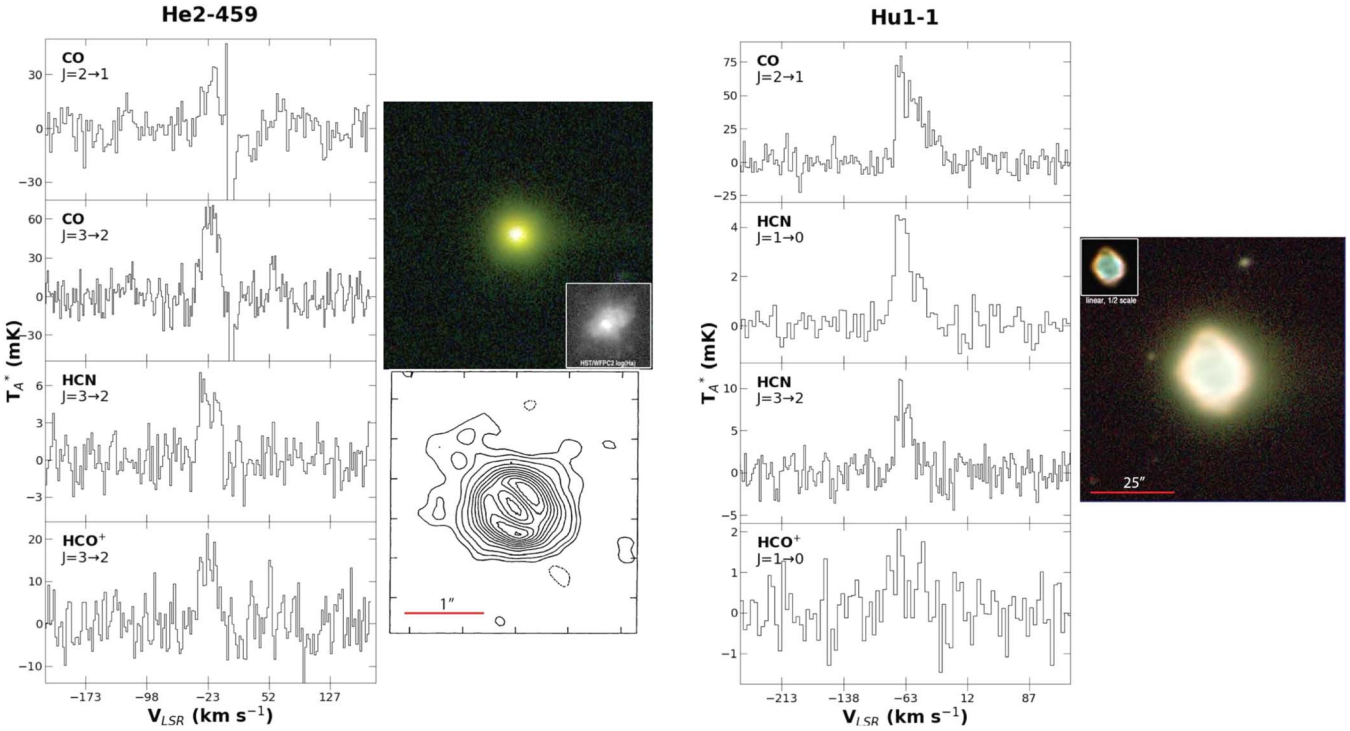

Figure 1. Spectra of HCN and HCO^+ detected in He 2-459 and Hu 1-1. CO spectra are also shown. The $J = 1 \rightarrow 0$ transitions of CO, HCN, and HCO^+ were measured with the ARO 12 m telescope at 0.625 MHz and smoothed to 1.25 MHz resolution; all other transitions were observed with the ARO SMT at 1 MHz resolution and smoothed to 2 MHz resolution. The temperature scale is T_A^*. Radio continuum and/or optical images of each nebula are also shown. Approximate spatial scales are indicated on the images. Vertical direction is north; left is east. The optical images from Manchado et al. (1996) have been colorized, with red representing log[N II], green log(Ha), and blue log[O III]. The inset for the He 2-459 image displays an HST/WFPC2 Ha log-scale image of the source, while that of Hu 1-1 is on a linear intensity scale. The VLA 8.4 GHz radio continuum map of He 2-459 by Kwok & Aaquist (1993) is also shown (synthesized beam $\sim 0\farcs2$).

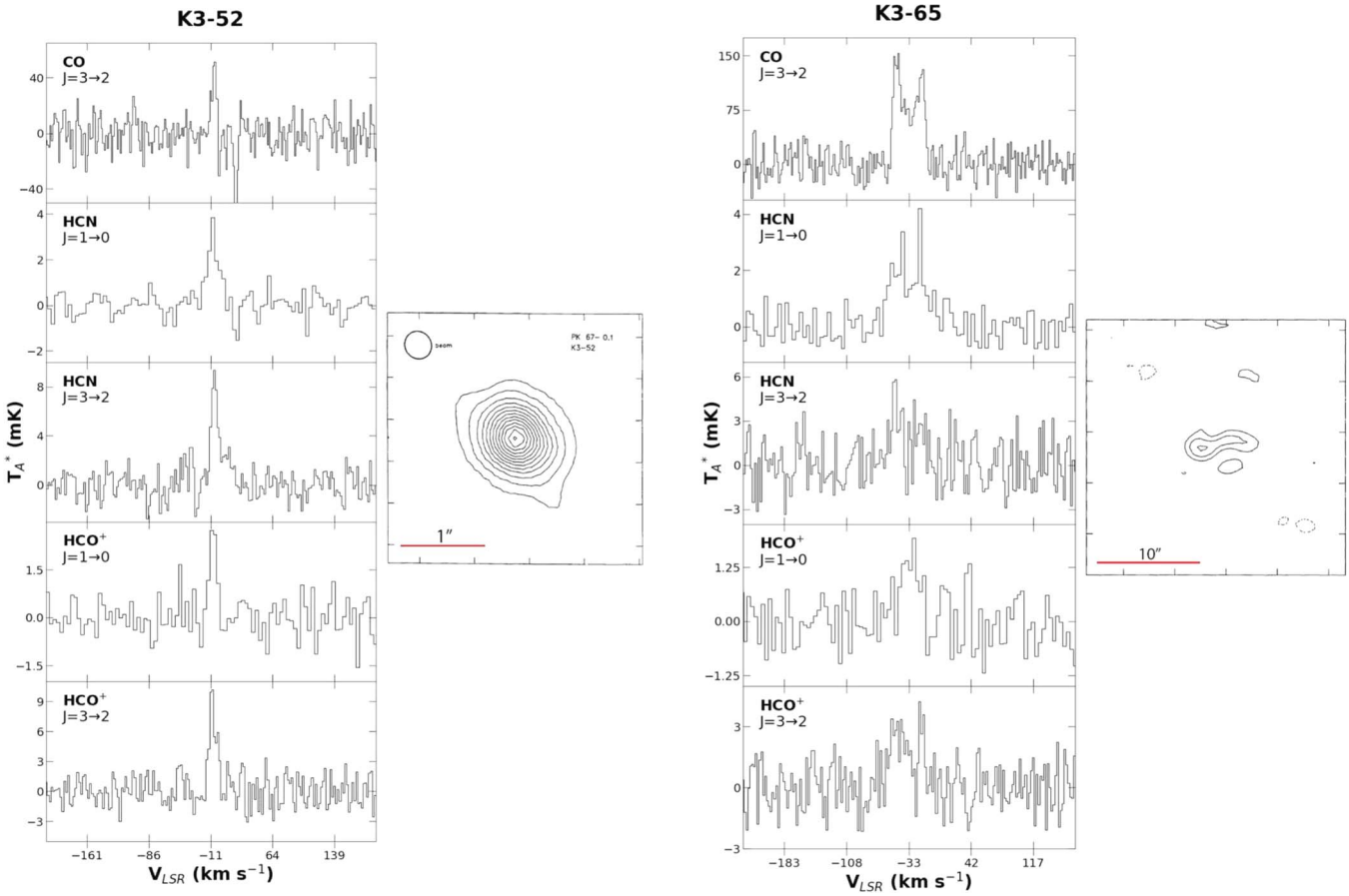

Figure 2. Same as Figure 1 for PNe K3-52 and K3-65. The VLA 5 GHz continuum images are shown from Aaquist & Kwok (1990).

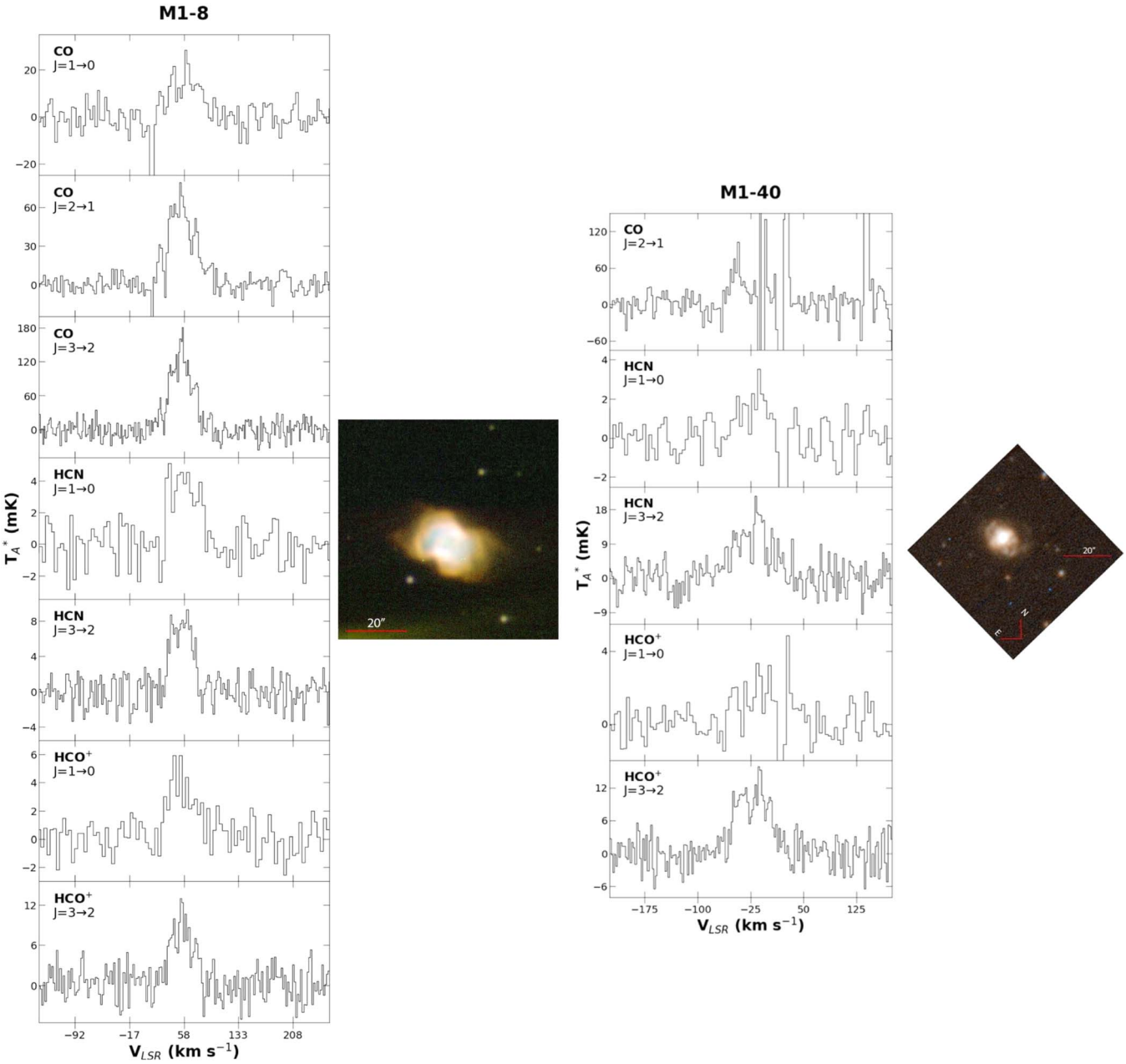

Figure 3. Same as Figure 1 for PNe M1-8 and M1-40. Optical images of both nebulae are presented. The image of M1-8 was obtained from Manchado et al. (1996; see Figure 1). In the image of M1-40 by Schwarz et al. (1992), red represents log(Ha+[N II]), blue log[O III], and green both.

41,100 yr, to be compared with our kinematic age of 12,530 yr, based on an expansion velocity of 17.5 km s^{-1}. It is apparently carbon-rich, with a C/O ratio of 1.8 (Bohigas 2008). We detected neither HCN nor HCO$^+$ in this PN with upper limits of <8–9 mK, peak to peak, for the $J = 3 \rightarrow 2$ lines. The $J = 2 \rightarrow 1$ line of CO was detected by Huggins et al. (2005), who noted that the line possessed a double-peaked profile. We also found a similar double-peaked profile in the CO $J = 3 \rightarrow 2$ transition, as shown in Figure 6.

Object M1-8 is a carbon-rich (C/O ∼ 2.5; Peimbert et al. 1995) PN. According to Ramos-Larios et al. (2008), it exhibits a bipolar structure with a central collimating disk. Its central star possesses the second-highest surface temperature of this sample (∼161,000 K; Kaler & Jacoby 1989). Stasińska et al. (1997) cited an evolutionary age of ∼16,100 yr; however, based on an angular size of 18″ (Phillips & Márquez-Lugo 2011), a distance of 3.06 kpc (Phillips & Márquez-Lugo 2011), and an expansion velocity of 39 km s^{-1} (half the average CO line width), we estimate a kinematic age of ∼3400 yr. The $J = 1 \rightarrow 0$ and $J = 3 \rightarrow 2$ transitions of HCN and HCO$^+$ were detected in this PN (Figure 3). The HCN profiles appear to have a box shape. Also shown in the figure are the $J = 1 \rightarrow 0$, $2 \rightarrow 1$, and $3 \rightarrow 2$ lines of CO, which show the possible presence of multiple velocity components, as also found by Huggins et al. (1996). Galactic contamination is present in the CO $J = 1 \rightarrow 0$ and possibly $J = 2 \rightarrow 1$ spectra.

Object M1-40 is a PN of uncertain morphology. Guzman-Ramirez et al. (2014) indicated a bipolar morphology in Hα, noting that the nebula exhibits a "clumpy doughnut-like structure" viewed head-on. Stanghellini et al. (1993), on the other hand, listed an irregular morphology for the nebula, while Corradi et al. (1998) classified it as elliptical. The source size is

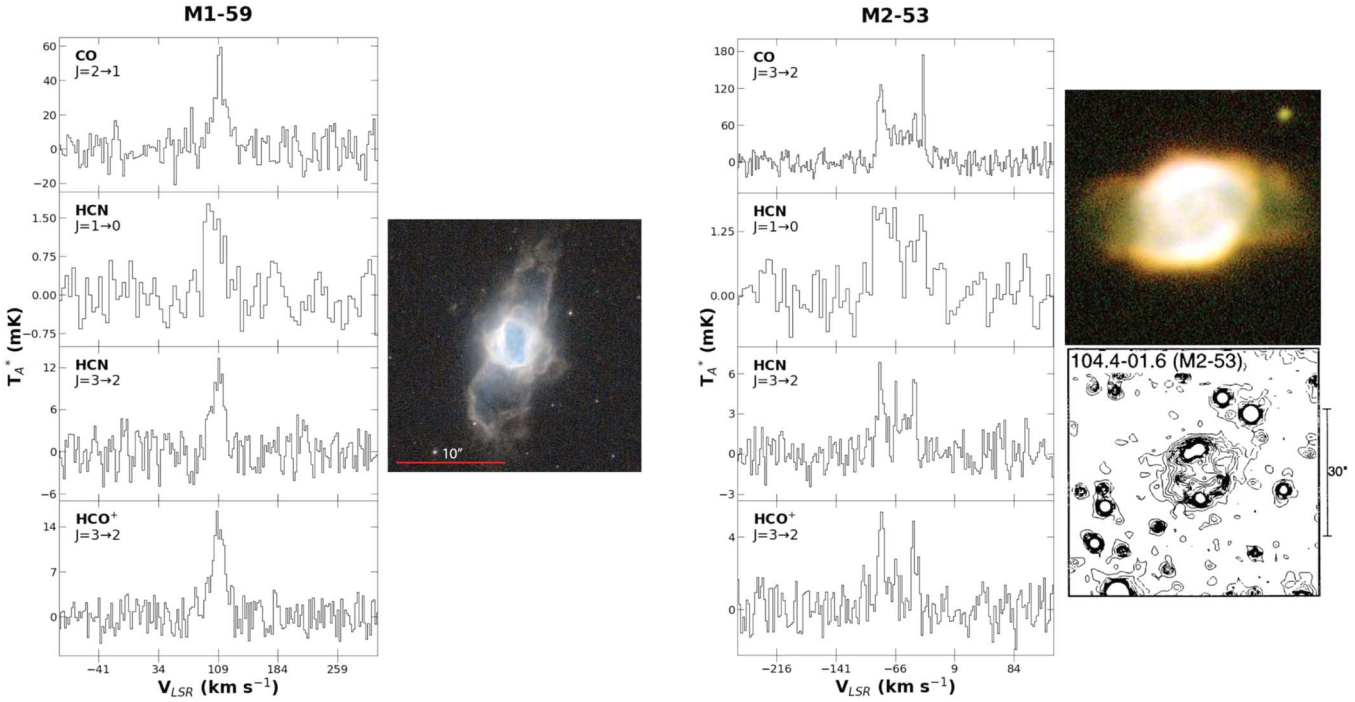

Figure 4. Same as Figure 1 for M1-59 and M2-53. Radio continuum and/or optical images of both nebulae are displayed. The optical image of M1-59 is from the HST/WFPC2 archives, with red representing log(F658N) (wavelength ∼658 nm), blue log(F656N) (wavelength ∼656 nm), and green both. The optical image of M2-53, at the top right, was originally published by Manchado et al. (1996; see Figure 1). The other is a *J*-band image from Saitō et al. (1999).

also uncertain. While it is given as 4.″8 by Phillips & Márquez-Lugo (2011), Hα and [O III] images from Schwarz et al. (1992) suggest a diameter closer to 20″. Here we adopt 10″ based on the optical image shown in Figure 3. Gesicki & Zijlstra (2007) reported a kinematic age of 1776 yr, in line with the kinematic age of 2580 yr we derived using a distance of 2.83 kpc (Phillips & Márquez-Lugo 2011) and an expansion velocity of 26 km s^{-1}. Both transitions of HCN and HCO$^+$ were detected in this source, although the $J = 1 \rightarrow 0$ lines have Galactic contamination, as does the CO $J = 2 \rightarrow 1$ spectrum (Figure 3). Huggins et al. (2005) indicated that the CO $J = 2 \rightarrow 1$ line had a "flat-topped profile" with significant Galactic contamination. Our profiles are broad and may be flat-topped.

Object M1-59 is a small (4.″8; Phillips & Márquez-Lugo 2011), middle-aged nebula. Hsia et al. (2014) reported a kinematic age of 4050 yr, consistent with our kinematic age of 4740 yr, derived using a distance of 3.54 kpc (Phillips & Márquez-Lugo 2011) and an expansion velocity of 8.5 km s^{-1}. The source is generally characterized as a bipolar nebula (e.g., Aaquist & Kwok 1990; Corradi et al. 1998; Guerrero et al. 2000). Specifically, Guerrero et al. (2000) described M1-59 as a bipolar PN with a "broad ring structure in the waist." However, the Hubble Space Telescope (HST) image published by Hsia et al. (2014) reveals an even more complex structure, with three pairs of bipolar lobes and a cavity or fourth lobe at the center. The H_2 2.12 μm emission from the lobes of the nebula was reported by Guerrero et al. (2000). In M1-59, both transitions of HCN were identified, as well as the $J = 3 \rightarrow 2$ transition of HCO$^+$; see Figure 4. The CO $J = 2 \rightarrow 1$ transition measured by Huggins et al. (2005) was described as a single component with broad wings; the wings are apparent in our CO line, and perhaps in HCN and HCO$^+$ as well.

Object M1-63 is a small (4.″2; Phillips & Márquez-Lugo 2011) PN of uncertain morphology. Guzman-Ramirez et al. (2018) classified it as elliptical, while Sahai et al. (2011) described it as bipolar with a complex substructure. Given a distance of 7.32 kpc (Phillips & Márquez-Lugo 2011) and an expansion velocity of 19 km s^{-1}, a kinematic age of 3840 yr was derived in this work. HCN and HCO$^+$ were not detected in this source. Our CO $J = 2 \rightarrow 1$ line is broad and flat-topped, as shown in Figure 6, while Huggins et al. (2005) found a double-peaked profile. Additionally, Guzman-Ramirez et al. (2018) reported the detection of CO $J = 3 \rightarrow 2$ with APEX, describing its line profile as complex, with three visible components.

Object M2-53 is an extremely carbon-rich PN with a C/O ratio of ∼4.7 (Bohigas 2008). These authors suggested that the nebula is an example of a type IIa PN with a progenitor mass of 2 $M_\odot$ based on its chemical makeup, and that the nebula exhibits an elliptical morphology. The central star temperature of this source is one of the hottest in our sample, at around 142,000 K (Kaler & Jacoby 1989); see Table 2. We derived an age of 6020 yr based on a size of 18″ (Phillips & Márquez-Lugo 2011), a distance of 3.64 kpc (Phillips & Márquez-Lugo 2011), and an expansion velocity of ∼25.8 km s^{-1} from CO. As shown in Figure 4, both transitions of HCN and the $J = 3 \rightarrow 2$ transition of HCO$^+$ were identified toward M2-53, along with the $J = 1 \rightarrow 0$ transition of HCN and the $J = 3 \rightarrow 2$ transition of CO. The line profiles suggest the presence of central, redshifted, and blueshifted components. The $J = 2 \rightarrow 1$ transition of CO of Huggins et al. (2005) exhibited a steep, double-peaked profile and some interstellar contamination in the redshifted part of the spectrum. Our CO $J = 3 \rightarrow 2$ transition looks very similar.

Object M4-17 is a relatively extended PN. Manchado et al. (1996) imaged the nebula in [N II], revealing a bipolar structure to the nebula with a well-defined ring. The size of the entire object was given as 24″, while the size of the ring itself was reported as 16″–20″, based on H_2 (Guerrero et al. 2000). Additionally, these authors noted the similarity between the

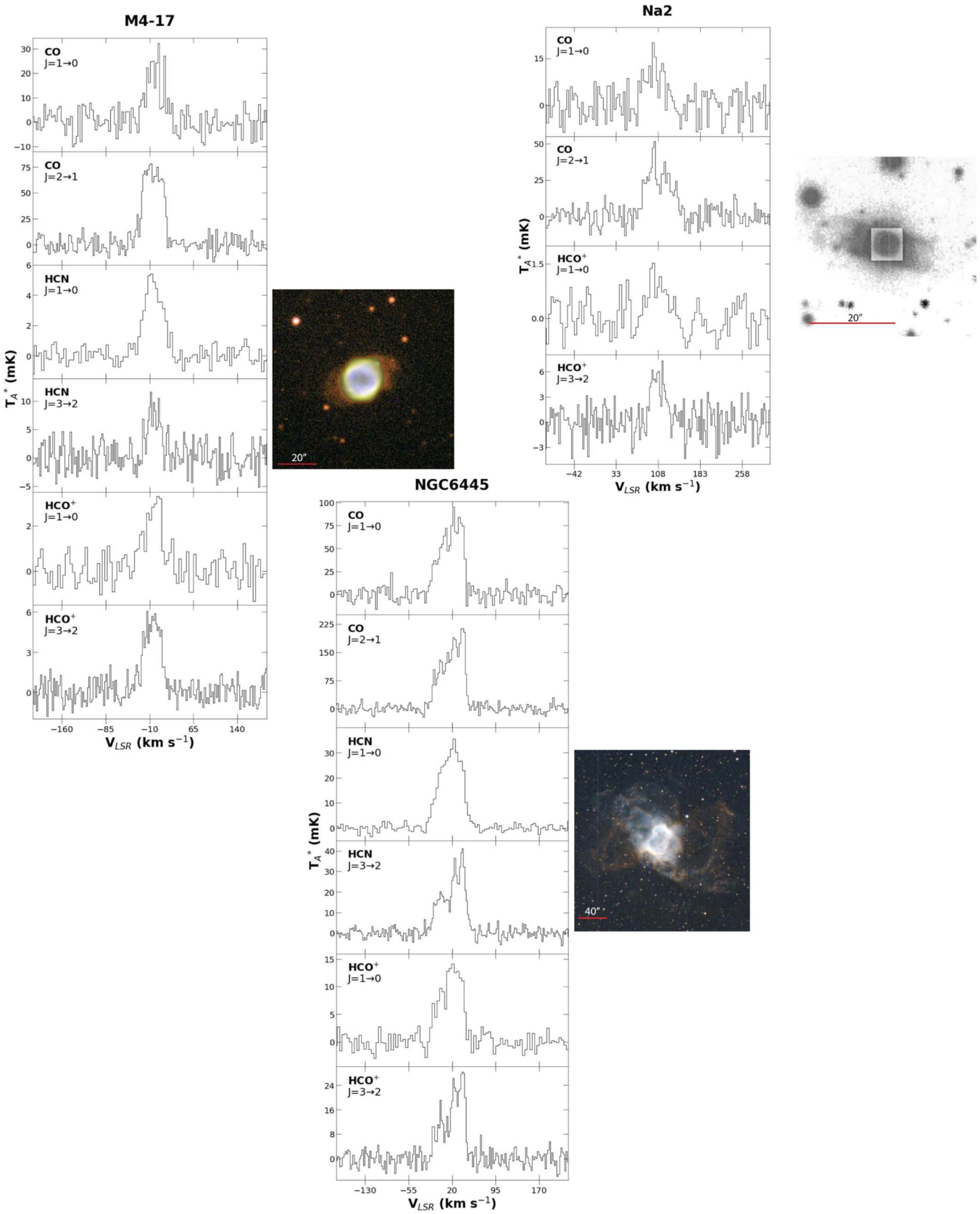

Figure 5. Same as Figure 1 for M4-17, Na 2, and NGC 6445. Optical images of each nebula are exhibited. That of M4-17 was obtained from Manchado et al. (1996), with red representing deep log(Ha), green log(Ha), and blue log[O III]. The [N II] image of Na 2 is from Corradi & Schwarz (1993). The image of NGC 6445 is from Schwarz et al. (1992); red represents log(Ha+[N II]), blue log[O III], and green both.

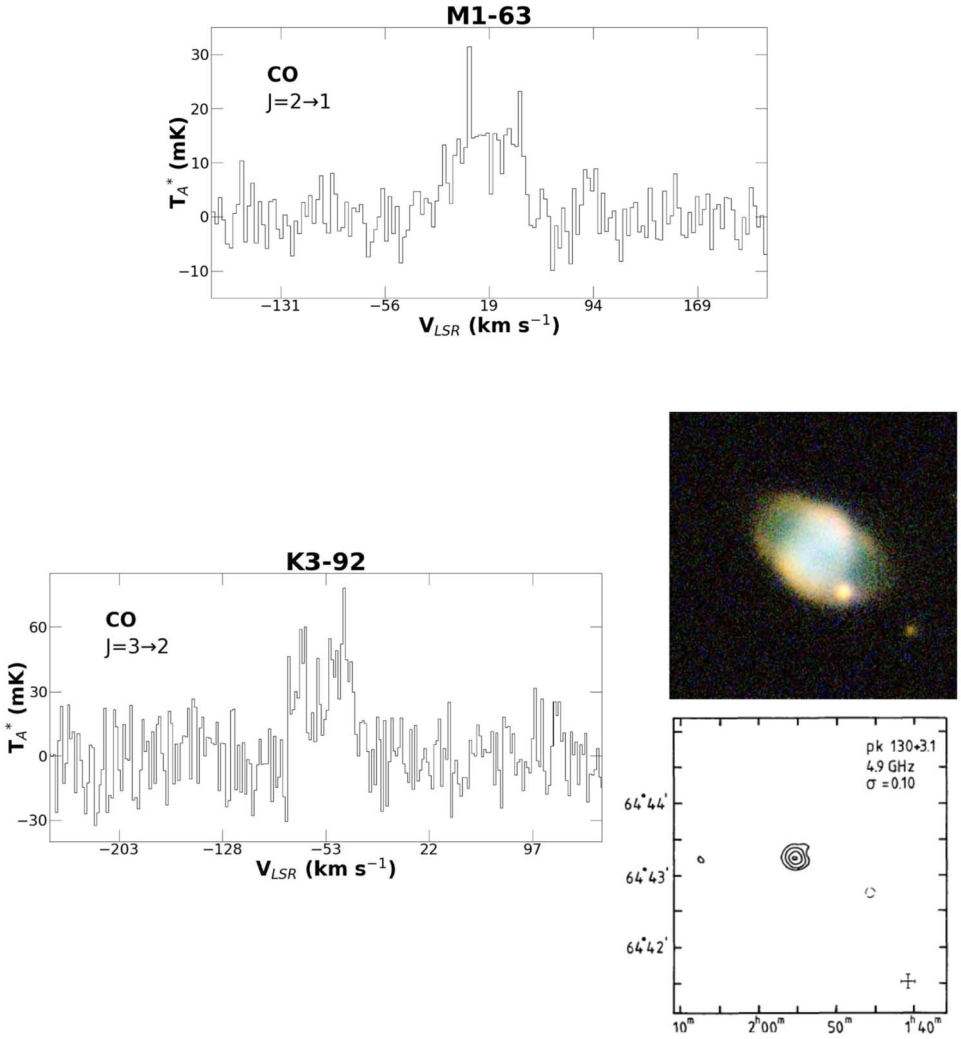

Figure 6. Same as Figure 1 for K3-92 and M1-63. The VLA 5 GHz map of K3-92 from Zijlstra et al. (1989) is shown, measured with a 10″ synthesized beam size. No optical or radio continuum images are available for M1-63.

optical and H_2 images in the ring and bipolar lobe structures. Assuming the angular size of 24″ from Manchado et al. (1996), a distance of 2.2 kpc (Guerrero et al. 2000), and an expansion velocity of 17.5 km s^{-1}, a kinematic age of 7160 yr was derived for M4-17. We detected both transitions of HCN and HCO^+ in this source, along with the $J = 1 \rightarrow 0$ and $J = 2 \rightarrow 1$ transitions of CO, as presented in Figure 5. Huggins et al. (2005) noted that the CO $J = 2 \rightarrow 1$ line possessed a flat-topped or concave profile, as found here.

Na 2 is a bipolar PN (Corradi & Schwarz 1993; Corradi & Schwarz 1995; Kastner et al. 1996; Corradi et al. 1998) about which little is known. Tylenda et al. (2003) estimated a source size of 6.″3 × 5.″7 based on Hα and [N II] observations. This extent is notably smaller than the 40″ of Corradi & Schwarz (1993), who included the faint extensions of the lobes in [N II] for their estimation. We adopt a size of 25″, excluding the faint emission. Given a distance of 9 kpc (Corradi & Schwarz 1993) and an expansion velocity of 18.8 km s^{-1}, we have estimated a kinematic age of 28,400 yr. Both the $J = 1 \rightarrow 0$ and $J = 3 \rightarrow 2$ lines of HCO^+ were detected in Na 2 (see Figure 5). In contrast, HCN was not seen. The $J = 1 \rightarrow 0$ and $J = 2 \rightarrow 1$ lines of CO were also observed. Huggins et al. (2005) found the CO $J = 2 \rightarrow 1$ line to have a double-peaked profile on top of a broader feature, consistent with our CO $J = 2 \rightarrow 1$ spectrum.

Also known as the Little Gem Nebula, NGC 6445 is a more extended (∼33″; Ortiz et al. 2011), middle-aged PN. Given a distance of 1.38 kpc (Stanghellini et al. 2008) and an expansion velocity of 23 km s^{-1}, a kinematic age of ∼4700 yr is estimated; a dynamical age of 3300 yr was derived by van Hoof et al. (2000). Unlike the other sources, HCN and HCO^+ was observed in NGC 6445 by Bublitz et al. (2019), who identified the $J = 1 \rightarrow 0$ lines of both molecules. We detected the $J = 1 \rightarrow 0$ and $J = 3 \rightarrow 2$ transitions of HCN and HCO^+, in addition to the $J = 1 \rightarrow 0$ and $J = 2 \rightarrow 1$ lines of CO; see Figure 5. Bublitz et al. (2019) noted that the lines were double-peaked; our profiles are similar, except our best fit to the spectra involves four velocity components (doublets of doublets), particularly evident in the $J = 1 \rightarrow 0$ and $J = 2 \rightarrow 1$ lines of CO. Because this source is considered to be multipolar, the four-component fit is justified and may correspond to two separate bipolar flows. The optical image suggests such a geometry as well. CN, OH, and OH^+ have also been identified in the nebula (Aleman et al. 2014; Bublitz et al. 2019).

4. Analysis

Column densities for CO, HCN, and HCO^+ were determined using RADEX, a non-LTE radiative transfer code described in

Table 3
Line Parameters for HCN, HCO^+, and CO

Source	Molecule	Transition	T_A^* (mK)	V_{LSR} (km s^{-1})	$\Delta V_{1/2}$ (km s^{-1})
He 2-459	HCN	$J = 3 \rightarrow 2$	6.0 ± 3.0	-21.0 ± 2.2	25.0 ± 2.2
	HCO^+	$J = 3 \rightarrow 2$	21.0 ± 10.0	-20.0 ± 2.2	24.0 ± 2.2
	CO	$J = 2 \rightarrow 1$[a]	~30	~−20	~25
		$J = 3 \rightarrow 2$[a]	65 ± 20	-20.0 ± 2.6	22.0 ± 2.6
Hu 1-1	HCN	$J = 1 \rightarrow 0$[b]	4.0 ± 1.0	~−68	~20
		$J = 3 \rightarrow 2$	10.0 ± 3.0	-65.3 ± 3.3	18.0 ± 3.3
	HCO^+	$J = 1 \rightarrow 0$	1.5 ± 1.0	-61.7 ± 8.4	30.0 ± 8.4
	CO	$J = 2 \rightarrow 1$[b]	75.0 ± 30.0	~−69	~30
K3-52	HCN	$J = 1 \rightarrow 0$	3.5 ± 1.0	-8.0 ± 4.2	12.6 ± 4.2
		$J = 3 \rightarrow 2$[c]	9.0 ± 2.0	-8.0 ± 2.2	10.0 ± 2.2
			~2	8.0 ± 2.2	12.0 ± 2.2
	HCO^+	$J = 1 \rightarrow 0$	2.5 ± 1.0	-8.8 ± 4.2	10.5 ± 4.2
		$J = 3 \rightarrow 2$	11.0 ± 3.0	-8.0 ± 2.2	12.0 ± 2.2
	CO	$J = 3 \rightarrow 2$[d]	53.0 ± 20.0	-6.5 ± 2.6	8.0 ± 2.6
K3-65	HCN	$J = 1 \rightarrow 0$	2.0 ± 1.0	-34.0 ± 8.4	43.0 ± 8.4
		$J = 3 \rightarrow 2$	4.0 ± 2.0	-32.0 ± 5.5	36.0 ± 5.5
	HCO^+	$J = 1 \rightarrow 0$	1.5 ± 1.0	-28.3 ± 8.4	32.3 ± 8.4
		$J = 3 \rightarrow 2$	3.0 ± 2.0	-33.0 ± 5.5	36.0 ± 5.5
	CO[a]	$J = 3 \rightarrow 2$	~160	~−32	~34
K3-92	CO[c]	$J = 3 \rightarrow 2$	67 ± 30	-43.0 ± 5.2	16.0 ± 5.2
			45 ± 30	-72.5 ± 5.2	12.0 ± 5.2
M1-8	HCN	$J = 1 \rightarrow 0$	4.0 ± 2.0	59.5 ± 4.2	40.0 ± 4.2
		$J = 3 \rightarrow 2$	8.0 ± 3.0	55.0 ± 3.3	40.5 ± 3.3
	HCO^+	$J = 1 \rightarrow 0$	5.0 ± 2.0	57.6 ± 4.2	40.2 ± 4.2
		$J = 3 \rightarrow 2$	13.0 ± 5.0	56.0 ± 3.3	37.3 ± 3.3
	CO	$J = 1 \rightarrow 0$[a]	20.0 ± 7.0	59.8 ± 3.3	42.4 ± 6.5
		$J = 2 \rightarrow 1$[d]	75.0 ± 10.0	54.1 ± 5.2	~40
		$J = 3 \rightarrow 2$	186.0 ± 40.0	56.5 ± 2.6	35.5 ± 2.6
M1-40	HCN	$J = 1 \rightarrow 0$[d]	2.0 ± 1.0	-24.1 ± 8.4	52.0 ± 8.4
		$J = 3 \rightarrow 2$	19.0 ± 8.0	-20.0 ± 5.5	52.0 ± 5.5
	HCO^+	$J = 1 \rightarrow 0$[d]	2.0 ± 1.0	-24.0 ± 8.4	52.0 ± 8.4
		$J = 3 \rightarrow 2$	16.0 ± 8.0	-20.0 ± 5.5	52.0 ± 5.5
	CO[a]	$J = 2 \rightarrow 1$	~50	~−20	…
M1-59	HCN	$J = 1 \rightarrow 0$	1.5 ± 1.0	105.0 ± 8.4	20.0 ± 8.4
		$J = 3 \rightarrow 2$	12.0 ± 5.0	110.0 ± 4.4	16.0 ± 4.4
	HCO^+	$J = 3 \rightarrow 2$	15.0 ± 5.0	110.0 ± 4.4	17.0 ± 4.4
	CO	$J = 2 \rightarrow 1$	50.0 ± 20.0	112.0 ± 5.5	17.0 ± 5.5
M1-63	CO	$J = 2 \rightarrow 1$	20.0 ± 10.0	19.0 ± 5.2	38.0 ± 5.2
M2-53[e]	HCN	$J = 1 \rightarrow 0$	1.7 ± 0.5	~−81	~34
			1.0 ± 0.5	~−40	~25
		$J = 3 \rightarrow 2$	6.0 ± 2.0	-84.3 ± 3.3	10.0 ± 3.3
			~2	~−60	…
			5.0 ± 2.0	-41.2 ± 3.3	5.0 ± 3.3
	HCO^+	$J = 3 \rightarrow 2$	4.0 ± 2.0	-83.0 ± 3.3	8.0 ± 3.3
			4.0 ± 2.0	-41.0 ± 3.3	8.0 ± 3.3
	CO	$J = 3 \rightarrow 2$	120.0 ± 20.0	-83.5 ± 2.6	10.0 ± 2.6
			~50	~−60	…
			75.0 ± 20.0	-41.0 ± 2.6	8.0 ± 2.6
M4-17	HCN	$J = 1 \rightarrow 0$	5.0 ± 1.0	-3.0 ± 4.2	36.0 ± 4.2
		$J = 3 \rightarrow 2$	10.0 ± 5.0	-3.0 ± 3.3	30.0 ± 3.3
	HCO^+	$J = 1 \rightarrow 0$	3.0 ± 1.0	-5.1 ± 4.2	37.8 ± 4.2
		$J = 3 \rightarrow 2$	6.0 ± 2.0	-4.0 ± 3.3	34.0 ± 3.3
	CO	$J = 1 \rightarrow 0$	27.0 ± 8.0	-4.0 ± 3.3	35.0 ± 3.3
		$J = 2 \rightarrow 1$	80.0 ± 15.0	-4.0 ± 3.9	35.0 ± 3.9
Na 2	HCO^+	$J = 1 \rightarrow 0$	1.5 ± 1.0	105.0 ± 10.0	40.0 ± 10.0
		$J = 3 \rightarrow 2$	7.0 ± 4.0	108.0 ± 6.0	30.0 ± 6.0
	CO	$J = 1 \rightarrow 0$	16.0 ± 5.0	102.0 ± 8.0	35.0 ± 8.0
		$J = 2 \rightarrow 1$	46.0 ± 10.0	110.0 ± 6.0	40.0 ± 6.0
NGC 6445[e]	HCN	$J = 1 \rightarrow 0$	23.0 ± 3.0	-0.2 ± 4.2	23.0 ± 4.2
			11.0 ± 3.0	11.8 ± 4.2	9.0 ± 4.2
			32.0 ± 3.0	23.3 ± 4.2	14.0 ± 4.2
			23.0 ± 3.0	37.8 ± 4.2	13.0 ± 4.2
		$J = 3 \rightarrow 2$	19.0 ± 5.0	-1.0 ± 2.2	20.0 ± 2.2

Table 3
(Continued)

Source	Molecule	Transition	T_A^* (mK)	V_{LSR} (km s^{-1})	$\Delta V_{1/2}$ (km s^{-1})
			10.0 ± 5.0	14.0 ± 2.2	12.0 ± 2.2
			33.0 ± 5.0	24.5 ± 2.2	8.0 ± 2.2
			42.0 ± 5.0	38.0 ± 2.2	12.0 ± 2.2
	HCO^+	$J = 1 \rightarrow 0$	8.0 ± 3.0	−0.5 ± 4.2	23.0 ± 4.2
			9.0 ± 3.0	16.0 ± 4.2	9.0 ± 4.2
			11.0 ± 3.0	26.5 ± 4.2	13.0 ± 4.2
			8.0 ± 3.0	37.5 ± 4.2	10.0 ± 4.2
		$J = 3 \rightarrow 2$	14.0 ± 5.0	−1.0 ± 3.3	20.0 ± 3.3
			8.0 ± 5.0	13.0 ± 3.3	6.0 ± 3.3
			25.0 ± 5.0	24.0 ± 3.3	9.0 ± 3.3
			30.0 ± 5.0	38.0 ± 3.3	12.0 ± 3.3
	CO	$J = 1 \rightarrow 0$	48.0 ± 12.0	−1.0 ± 3.3	23.0 ± 3.3
			31.0 ± 12.0	10.0 ± 3.3	6.0 ± 3.3
			83.0 ± 12.0	22.5 ± 3.3	12.0 ± 3.3
			74.0 ± 12.0	36.0 ± 3.3	11.0 ± 3.3
		$J = 2 \rightarrow 1$	126.0 ± 30.0	0.0 ± 2.6	22.0 ± 2.6
			66.0 ± 30.0	12.5 ± 2.6	6.0 ± 2.6
			175.0 ± 30.0	25.0 ± 2.6	13.0 ± 2.6
			221.0 ± 30.0	39.0 ± 2.6	10.0 ± 2.6

Notes.
[a] Strong Galactic contamination.
[b] Asymmetric profile; redshifted wing (see text).
[c] Two-component fit.
[d] Weak Galactic contamination.
[e] Complex profile; possible multiple velocity components (see text).

van der Tak et al. (2007). Given an assumed kinetic temperature, H_2 density, and molecular column density, RADEX utilizes the Sobolev escape probability method to solve the equation of radiative transfer and produce molecular line intensities that may then be compared to the measured values. The kinetic temperature, H_2 number density, and column density may be varied in order to determine the set of parameters that best reproduce the observations.

In most cases, no more than two transitions were detected per molecule. Thus, the kinetic temperature was held constant at $T_K = 20$ K, a typical temperature for molecular gas in most PNe, although there are cases where it is higher (e.g., Zack & Ziurys 2013; Edwards & Ziurys 2014; Edwards et al. 2014). The H_2 densities determined in the analysis were typically in the range of ~ 0.2–14×10^6 cm^{-3} for HCN and HCO^+, though several of the densities estimated via the CO modeling were notably lower, on the order of $\sim 10^3$–10^4 cm^{-3}. In several instances, only one transition of a given molecule (such as HCN) was detected. In this case, the H_2 density was held constant to the value found from one of the other molecules observed in that source for which two transitions were measured. For CO in M1-8, three transitions were detected, enabling all three parameters to be varied, yielding a kinetic temperature of 60 K and $n(H_2) = 10^6$ cm^{-3}. This kinetic temperature was used to fit HCN and HCO^+ for this source. Note that the temperature for M1-8 is higher than 20 K, but some PNe have higher values, such as NGC 6537, which has $T_K \sim 60$ K (Edwards & Ziurys 2013).

In the analysis, the brightness temperatures were corrected only for source size, as listed in Table 2. In more extended sources, the computations were also carried out assuming a "clump filling factor" (see Schmidt & Ziurys 2016). This factor accounts for molecular material being contained in knots, based on those observed in H_2 in the Helix Nebula (Meixner et al. 2005). These authors found that a value of 0.2 was appropriate.

Molecular column densities were varied between 10^{10} and 10^{15} cm^{-2} for HCN and HCO^+ and between 10^{15} and 10^{20} cm^{-2} for CO to find the best match to the observational data. When appropriate, the H_2 number density was varied between 10^3 and 10^7 cm^{-3}. The resultant column densities for CO, HCN, and HCO^+, as well as the corresponding H_2 densities, are shown in Table 4. The column densities fall within the ranges $N_{tot}(CO) = 0.007$–3.8×10^{17}, $N_{tot}(HCO^+) = 0.008$–9.5×10^{13}, and $N_{tot}(HCN) = 0.005$–1.1×10^{14} cm^{-2}. For the extended sources, assuming a clumping factor, the column densities are factors of 3–4 higher, with $N_{tot}(CO) = 0.02$–5.9×10^{17}, $N_{tot}(HCN) = 0.2$–6.5×10^{13}, and $N_{tot}(HCO^+) = 0.03$–3.3×10^{13} cm^{-2}.

H_2 column densities were not available from the literature for any of the sources in this work; therefore, fractional abundances relative to H_2 were derived from CO, assuming $CO/H_2 \sim 10^{-4}$. This ratio is typical for PNe (e.g., Healy & Huggins 1990; Huggins et al. 2002; Zack & Ziurys 2013; Edwards et al. 2014). The resultant fractional abundances are $f(HCN) \sim 0.2$–1.5×10^{-7} and $f(HCO^+) \sim 0.3$–5.1×10^{-8} (see Table 4).

5. Discussion

5.1. Polyatomic Molecules in PNe

In their 2016 work, Schmidt & Ziurys detected either HCN or HCO^+ in 13 out of 17 PNe, or 77%, based on their $J = 1 \rightarrow 0$ and $J = 3 \rightarrow 2$ transitions. Both molecules were not always observed in every source, such that the detection rate per molecule was 65%. In this survey of 13 sources, either

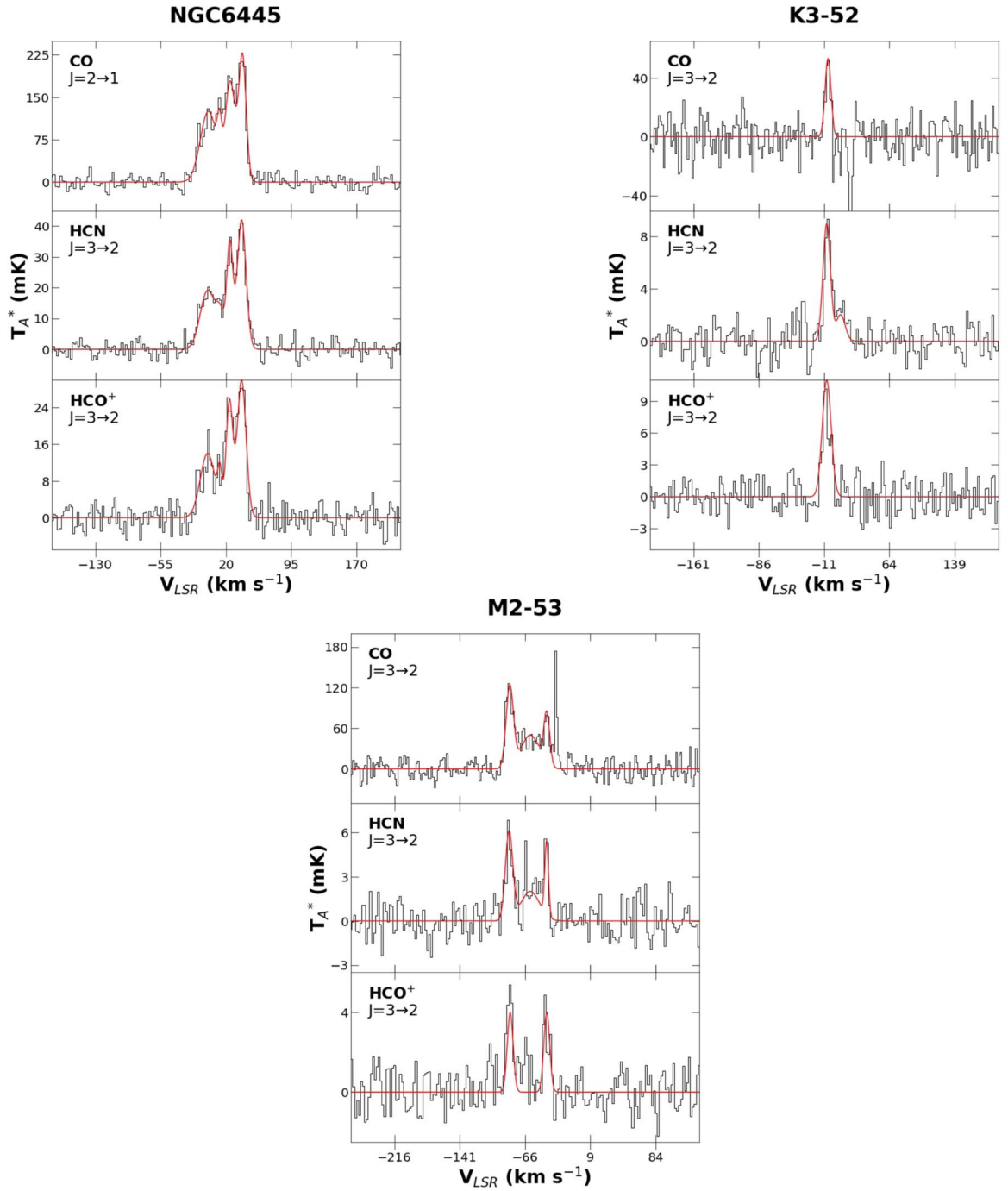

Figure 7. Representative fits to CO, HCN, and HCO^+ spectra for NGC 6445, K3-52, and M2-53. For K3-52, one additional component was used to fit a smaller feature on the redward side of the main component of the HCN $J = 3 \rightarrow 2$ line. Four components were modeled for the spectra in NGC 6445, while two to three components were applied for all lines in M2-53. The fits are overlaid in red atop the associated spectra for each transition.

HCN or HCO^+ was identified in 11 of the nebulae, a detection rate of 85%. Individually, HCN was identified in 10 sources, or 77% of the target list, and HCO^+ was detected in 11, or 85%. Both were identified in 10 objects (77%). In the course of other studies, both HCN and HCO^+ have been found in six other nebulae: NGC 7027 and the Helix (NGC 7293), Ring (NGC 6720), Red Spider (NGC 6537), and Dumbbell (NGC 6853) nebulae, as well as M2-48 (Bachiller et al. 1997; Zhang et al. 2008; Edwards & Ziurys 2013, 2014; Zack & Ziurys 2013; Edwards et al. 2014; Bublitz et al. 2019; Schmidt et al. 2018b). In total, polyatomic molecules in the guise of either HCN or HCO^+ have been detected in 30 out of 36 PNe, or 83%, given this total sample. Both species have been found in 71% of the 35 objects. Therefore, based on this sample, polyatomic molecules, or at least triatomic species, are common in PNe.

Overall, the abundances of HCN and HCO^+ do not vary significantly among these nebulae, although there are small differences. In their survey, Schmidt & Ziurys (2016) found $f(\mathrm{HCN}) \sim 0.1\text{–}9.1 \times 10^{-7}$ and $f(\mathrm{HCO^+}) \sim 0.04\text{–}7.4 \times 10^{-7}$. Toward M2-48, the Helix, and the Red Spider Nebula, HCN had abundances in the range $f(\mathrm{HCN}) \sim 0.2\text{–}1.2 \times 10^{-7}$, while for HCO^+, these sources displayed $f(\mathrm{HCO^+}) \sim 0.14\text{–}1 \times 10^{-7}$

Table 4
Column Densities and Fractional Abundances

Source	Molecule	$n(H_2)$ (cm^{-3})	Column Density (cm^{-2})	$f(X/H_2)$
He 2-459	HCN	9×10^{6a}	$5.6 \pm 1.3 \times 10^{13}$	1.5×10^{-8}
	HCO^+	9×10^{6a}	$9.5 \pm 3.8 \times 10^{13}$	2.5×10^{-8}
	CO	9×10^{6}	$\sim 3.8 \times 10^{17}$	
Hu 1-1	HCN	2×10^{6}	$6.4 \pm 1.2 \times 10^{12}$	3.0×10^{-8}
	HCO^+	2×10^{6b}	$3.2 \pm 0.6 \times 10^{12}$	1.5×10^{-8}
	CO	2×10^{6b}	$2.1 \pm 0.5 \times 10^{16}$	
K3-52	HCN	2×10^{6}	$1.1 \pm 0.4 \times 10^{14}$	7.9×10^{-8}
	HCO^+	7×10^{5}	$4.3 \pm 1.6 \times 10^{13}$	3.1×10^{-8}
	CO	1×10^{6b}	$\sim 1.4 \times 10^{17}$	
K3-65	HCN	2×10^{6}	$2.5 \pm 0.9 \times 10^{13}$	1.7×10^{-8}
	HCO^+	3×10^{5}	$9.3 \pm 4.2 \times 10^{12}$	6.2×10^{-9}
	CO	1×10^{6b}	$\sim 1.5 \times 10^{17}$	
M1-8	HCN	7×10^{5}	$3.8 \pm 1.1 \times 10^{12}$	2.4×10^{-8}
	HCO^+	2×10^{5}	$2.7 \pm 0.7 \times 10^{12}$	1.7×10^{-8}
	CO	1×10^{6}	$1.6 \pm 0.3 \times 10^{16}$	
M1-40	HCN	1×10^{7}	$1.3 \pm 0.4 \times 10^{13}$	5.4×10^{-8}
	HCO^+	2×10^{6}	$6.9 \pm 2.3 \times 10^{12}$	2.9×10^{-8}
	CO	8×10^{6b}	$\sim 2.4 \times 10^{16}$	
M1-59	HCN	8×10^{6b}	$1.4 \pm 0.7 \times 10^{13}$	4.0×10^{-8}
	HCO^+	8×10^{6b}	$6.6 \pm 2.0 \times 10^{12}$	1.9×10^{-8}
	CO	8×10^{6b}	$3.5 \pm 1.4 \times 10^{16}$	
M2-53 -80 km s^{-1}	HCN	4×10^{6}	$1.2 \pm 0.2 \times 10^{12}$	3.9×10^{-8}
	HCO^+	4×10^{6b}	$8.3 \pm 3.9 \times 10^{10}$	2.7×10^{-9}
	CO	4×10^{6b}	$3.1 \pm 0.7 \times 10^{15}$	
–40 km s^{-1}	HCN	6×10^{6}	$5.2 \pm 1.5 \times 10^{11}$	3.5×10^{-8}
	HCO^+	6×10^{6b}	$8.0 \pm 3.7 \times 10^{10}$	5.3×10^{-9}
	CO	6×10^{6b}	$\sim 1.5 \times 10^{15}$	
M4-17	HCN	3×10^{6}	$2.7 \pm 0.6 \times 10^{12}$	4.5×10^{-8}
	HCO^+	5×10^{5}	$1.0 \pm 0.3 \times 10^{12}$	1.7×10^{-8}
	CO	9×10^{3}	$6.0 \pm 1.1 \times 10^{15}$	
Na 2	HCO^+	1×10^{6}	$5.7 \pm 2.4 \times 10^{11}$	1.6×10^{-8}
	CO	8×10^{3}	$3.5 \pm 0.8 \times 10^{15}$	
NGC 6445 0 km s^{-1}	HCN	1×10^{6}	$4.1 \pm 0.6 \times 10^{12}$	9.8×10^{-8}
	HCO^+	5×10^{5}	$9.2 \pm 2.6 \times 10^{11}$	2.2×10^{-8}
	CO	9×10^{3}	$4.2 \pm 0.8 \times 10^{15}$	
12 km s^{-1}	HCN	2×10^{6}	$9.7 \pm 3.0 \times 10^{11}$	1.5×10^{-7}
	HCO^+	3×10^{5}	$3.3 \pm 1.4 \times 10^{11}$	5.1×10^{-8}
	CO	6×10^{3}	$6.5 \pm 3.1 \times 10^{14}$	
23 km s^{-1}	HCN	2×10^{6}	$3.0 \pm 0.6 \times 10^{12}$	8.3×10^{-8}
	HCO^+	7×10^{5}	$6.9 \pm 2.2 \times 10^{11}$	1.9×10^{-8}
	CO	6×10^{3}	$3.6 \pm 1.2 \times 10^{15}$	
38 km s^{-1}	HCN	3×10^{6}	$2.8 \pm 0.5 \times 10^{12}$	8.5×10^{-8}
	HCO^+	1×10^{6}	$5.9 \pm 1.8 \times 10^{11}$	1.8×10^{-8}
	CO	1.5×10^{4}	$3.3 \pm 0.7 \times 10^{15}$	

Notes.
[a] Held fixed to value for CO.
[b] Held fixed to value for HCN, HCO^+, or average of the two.

(Edwards & Ziurys 2013, 2014; Zeigler et al. 2013; Schmidt & Ziurys 2017a). Considering the complete ranges, these values differ from those found in this survey ($f(HCN) \sim 0.2$–1.5×10^{-7} and $f(HCO^+) \sim 0.3$–5.1×10^{-8}) by no more than factors of 2–6.

5.2. Constant Abundances across Nebular Age

There are few available models of the chemistry in PNe. The most recent model by Redman et al. (2003) studied the molecular composition of PNe, assuming the formation of clumps early in the nebular history, thus protecting molecular material from destructive UV radiation from the central white dwarf. In general, the authors found that molecular abundances decreased over the course of the ~10,000 yr life span of a PN, typically dropping by 3–5 orders of magnitude. This decrease may result from the assumed $t^{-3/2}$ density dependence of the clumps, where t = time. The clumps therefore disperse rather quickly. However, as our observations of the Helix have showed, densities in the clumps can remain quite high, even at the late stages of PNe (Zack & Ziurys 2013).

In contrast, observational data suggested no catastrophic decline in molecular abundance. Bachiller et al. (1997), in earlier work, proposed that a range of molecular species (CN, HCH, HCO^+, and HNC) could survive in the advanced stages of the PN phase, primarily based on observations of the Helix and the Ring. Tenenbaum et al. (2009) also proposed molecular survival in the late PN phase after detecting CCH, c-C_3H_2, and H_2CO in the Helix. In 2014, Edwards et al. found a negligible decrease in the abundances of CO, CS, and HCO^+ in five PNe spanning an age range of ~10,000 yr. Schmidt & Ziurys (2016) greatly expanded the number of PNe observed and discovered that, within this enlarged sample, the abundances of HCN and HCO^+ remained fairly constant from 700 to 12,000 yr.

The detection of HCN and HCO^+ in 10 and 11 new PNe, respectively, have provided yet further evidence for the persistence of polyatomic molecules across the entire nebula life span. Figure 8 summarizes the results for 30 PNe for which HCO^+ and HCN have been measured to date, plotting fractional abundances for each molecule with respect to molecular hydrogen as a function of nebular age. Red and blue circles reflect values previously reported for HCN and HCO^+, respectively (from Zack & Ziurys 2013; Edwards et al. 2014; Schmidt & Ziurys 2016, 2017a), while red and blue stars illustrate the HCN and HCO^+ abundances presented in this work. The magenta and cyan triangles depict the predictions of the Redman et al. (2003) model for HCN and HCO^+, respectively, at three epochs: 2550, 6300, and 10,000 yr. As seen in the figure, over this time span, the model predicts a significant depletion in the abundance of HCN (~7 orders of magnitude); the observed values, in contrast, lie within factors of 10–100 of one another across this time span. The HCO^+ abundance is not predicted to decrease as dramatically as HCN; however, the model estimates are significantly lower than the observed values at all epochs. As mentioned, the decrease in abundance results from the lack of shielding in the clumps. The assumed time $t^{-3/2}$ density dependence of the clumps may be too severe. Rather, the clumps appear to maintain higher densities longer than the models predict (e.g., Zack & Ziurys 2013; Schmidt & Ziurys 2016, 2017a).

The results of the 30 nebulae represented in Figure 8 definitively indicate that, contrary to the predictions of chemical models, there is no notable temporal variation in HCN or HCO^+ abundances over the course of the ~10,000–20,000 yr nebular lifespan. Other works indicate that the same holds true for other molecular species, including HNC and CCH (e.g., Schmidt & Ziurys 2017a, 2017b). These results suggest that the clumps within which molecules are expected to reside in PNe are more effective at shielding this material than expected, based on the models. Further, as noted by Schmidt & Ziurys (2016), Schmidt et al. (2018a), and Ziurys (2019), these abundances are generally higher by 1–2

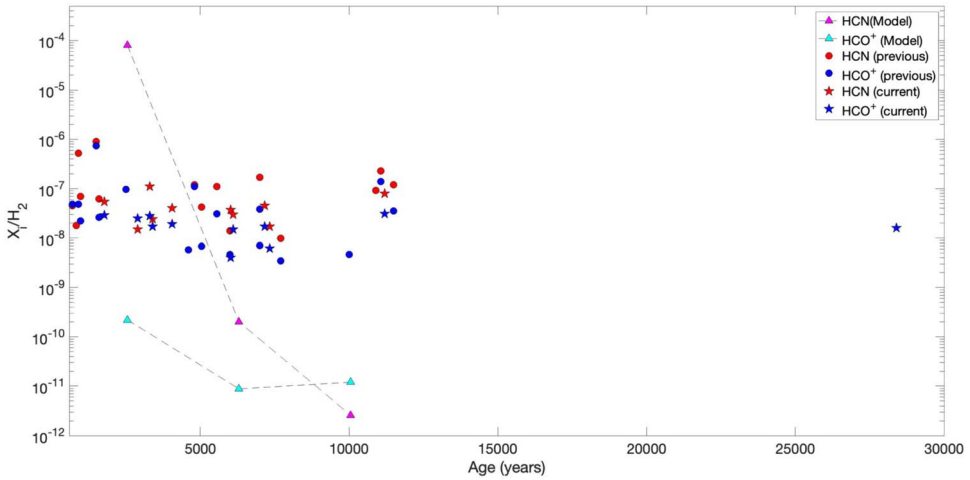

Figure 8. Plot of fractional abundances of HCN and HCO^+ vs. nebular age (in years) for 30 PNe from this study and the literature. Red and blue stars represent the abundances presented in this work; red and blue circles indicate abundances reported by Schmidt & Ziurys (2016), Zhang et al. (2008; NGC 7027), Edwards & Ziurys (2013; NGC 6537), Edwards & Ziurys (2014; M2-48), Schmidt & Ziurys (2017a) and Zack & Ziurys (2013; NGC 7293), and Edwards et al (2014; NGC 6720 and NGC 6853). Average abundances were used for sources with multiple velocity components. The magenta and cyan triangles depict the model abundances of Redman et al. (2003) for HCN and HCO^+, respectively, at three different epochs. This figure demonstrates that, in stark contrast to model predictions, the HCN and HCO^+ abundances do not significantly vary with nebular age.

orders of magnitude than those reported for diffuse clouds. For example, HCN and HCO^+ have typical abundances of $\sim 10^{-9}$ in diffuse gas (e.g., Liszt & Lucas 2001). Taken together, this evidence strongly insinuates that the polyatomic molecules observed in diffuse clouds originate from the ejecta of PNe. The globules that shield the molecular material in PNe from photodestruction disperse into the surrounding ISM, seeding it with molecular material (see Tenenbaum et al. 2009). Such a mechanism would explain the presence of polyatomic molecules in diffuse clouds, whose in situ formation is problematic given the low densities of these environments (Snow & McCall 2006).

5.3. Impact on Morphology and the C/O Ratio

The C/O ratio is only available for five of the 13 target nebulae: Hu 1-1, K3-92, M1-8, M2-53, and NGC 6445 (see Table 2). Four of these are carbon-rich, and the fifth, NGC 6445, has a C/O ratio of $\sim$1. Both HCN and HCO^+ were detected in four of these nebulae, except for K3-92, where only CO was observed. Based on this limited sample, a tentative conclusion might be drawn that the molecular content of PNe is enhanced in sources where $C/O \geqslant 1$. This scenario is certainly the case for circumstellar envelopes of evolved stars (see Tenenbaum et al. 2010). Because such envelopes evolve to PNe, perhaps this result is not surprising. However, additional C/O ratios need to be measured in PNe before a definitive conclusion can be made.

The nebulae in this survey are predominantly bipolar or multipolar. Only a few PNe are definitively classified as elliptical or irregular: Hu 1-1, K3-92, and M2-53. There is also some debate as to the classification of several nebulae, including M1-63, which is labeled as either elliptical or bipolar (Sahai et al. 2011; Guzman-Ramirez et al. 2018). The optical image of M2-53 suggests it is actually bipolar (see Figure 4).

Nearly all of the PNe that showed evidence of HCN and/or HCO^+ emission are bipolar/multipolar, aside from Hu 1-1, which is elliptical. The two nebulae where no detections of either molecule occurred, K3-92 and M1-63, are potentially elliptical sources. Schmidt & Ziurys (2016) observed a similar phenomenon. No HCN or HCO^+ detections were made in four nebulae, three of which were elliptical. There may be a strong connection between the presence of polyatomic molecules and bipolar morphology that merits further investigation.

H_2 emission has long been associated with bipolar nebulae, but is not exclusive to them (e.g., Guerrero et al. 2000). Bipolar PNe tend to be brighter in H_2 than those of other morphological types (Marquez-Lugo et al. 2013). The origin of the connection between bipolar morphology and H_2 emission is still unclear. It has been suggested that the relatively dense equatorial regions of bipolar PNe provide a refuge for molecular material by dust and self-shielding, thus leading to the bias in H_2 detections (Kastner et al. 1996; Guerrero et al. 2000). Indeed, Woods et al. (2005) suggested that the lack of detection of many molecular lines in two protoplanetary nebulae results from the lack of dense tori in these sources. The dominance of molecular detections in bipolar nebulae appears to hold true beyond H_2.

6. Conclusions

This survey provides additional evidence that polyatomic molecules are common constituents of PNe, regardless of nebular age. With this work, HCN and HCO^+ have now been identified in $\sim$30 PNe; this study also extends the apparent upper age limit from 12,000 to 28,000 yr. The observed abundances of HCN and HCO^+ across the life span of PNe are not reproduced in current chemistry models. Over these $\sim$30 sources, the determined abundances are 1–2 orders of magnitude higher that those measured in diffuse clouds, consistent with the seeding of the diffuse ISM with molecule-rich PN ejecta. The nebulae in which HCN and/or HCO^+ are detected are predominantly bipolar, as found for H_2. Overall, this work reveals an additional set of nebulae worthy of further study and indicates that future molecular surveys of PNe are likely to be successful.

This research was supported by NSF grants AST-1907910 and AST-1531366. The authors thank E. F. Lauria for providing an excellent new receiver system for the ARO 12 m.

ORCID iDs

D. R. Schmidt https://orcid.org/0000-0001-7519-6819
K. R. Gold https://orcid.org/0000-0002-6830-6239
L. M. Ziurys https://orcid.org/0000-0002-1805-3886

References

Aaquist, O. B., & Kwok, S. 1990, A&AS, 84, 229
Acker, A., & Neiner, C. 2003, A&A, 403, 659
Aleman, I., Ueta, T., Ladjal, D., et al. 2014, A&A, 566, A79
Bachiller, R., Forveille, T., Huggins, P. J., & Cox, P. 1997, A&A, 324, 1123
Bohigas, J. 2001, RMxAA, 37, 237
Bohigas, J. 2008, ApJ, 674, 954
Bublitz, J., Kastner, J. H., Standander-García, M., et al. 2019, A&A, 625, A101
Cami, J., Bernard-Salas, J., Peeters, E., & Malek, S. E. 2010, Sci, 329, 1180
Corradi, R. L. M., Aznar, R., & Mampaso, A. 1998, MNRAS, 297, 617
Corradi, R. L. M., & Schwarz, H. E. 1993, A&A, 278, 247
Corradi, R. L. M., & Schwarz, H. E. 1995, A&A, 293, 871
Delgado-Inglada, G., & Rodríguez, M. 2014, ApJ, 784, 173
Edwards, J. L., Cox, E. G., & Ziurys, L. M. 2014, ApJ, 791, 79
Edwards, J. L., & Ziurys, L. M. 2013, ApJL, 770, L5
Edwards, J. L., & Ziurys, L. M. 2014, ApJL, 794, L27
García-Hernández, D. A., Iglesias-Groth, S., Acosta-Pulido, J. A., et al. 2011, ApJL, 737, L30
García-Hernández, D. A., Manchado, A., García-Lario, P., et al. 2010, ApJL, 724, L39
García-Hernández, D. A., Villaver, E., García-Lario, P., et al. 2012, ApJ, 760, 107
Gesicki, K., & Zijlstra, A. A. 2007, A&A, 467, L29
Guerrero, M. A., Villaver, E., Manchado, A., Garcia-Lario, P., & Prada, F. 2000, ApJS, 127, 125
Guzman-Ramirez, L., Gómez-Ruíz, A. I., Boffin, H. M. J., et al. 2018, A&A, 618, A91
Guzman-Ramirez, L., Lagadec, E., Jones, D., Zijlstra, A. A., & Gesicki, K. 2014, MNRAS, 441, 364
Healy, A. P., & Huggins, P. J. 1990, AJ, 100, 511
Hora, J. L., Latter, W. B., & Deutsch, L. K. 1999, ApJSS, 124, 195
Hsia, C.-H., Chau, W., Zhang, Y., & Kwok, S. 2014, ApJ, 787, 25
Huggins, P. J., Bachiller, R., Cox, P., & Forveille, T. 1996, A&A, 315, 284
Huggins, P. J., Bachiller, R., Planesas, P., Forveille, T., & Cox, P. 2005, ApJS, 160, 272
Huggins, P. J., Forveille, T., Bachiller, R., et al. 2002, ApJL, 573, L55
Huggins, P. J., & Healy, A. P. 1989, ApJ, 346, 201
Kaler, J. B., & Jacoby, G. H. 1989, ApJ, 345, 871
Kastner, J. H., Weintraub, D. A., Galten, I., Merrill, K. M., & Probst, R. G. 1996, ApJ, 462, 777
Kwok, S., & Aaquist, O. B. 1993, PASP, 105, 1456
Liszt, H., & Lucas, R. 2001, A&A, 370, 576
Manchado, A., Guerrero, M. A., Stanghellini, L., & Serra-Ricart, M. 1996, The IAC Morphological Catalog of Northern Galactic Planetary Nebulae (La Laguna: Instituto de Astrofisica de Canarias)
Marquez-Lugo, R. A., Ramos-Larios, G., Guerrero, M. A., & Vázquez, R. 2013, MNRAS, 429, 973
Meixner, M., McCullough, P., Hartman, J., Son, M., & Speck, A. 2005, AJ, 130, 1784
Neufeld, D., Goto, M., Geballe, T. R., et al. 2020, ApJ, 894, 37
Ortiz, R., Copetti, M. V. F., & Lorenz-Martins, S. 2011, MNRAS, 418, 2004
Otsuka, M., Kemper, F., Hyung, S., et al. 2013, ApJ, 764, 77
Parker, Q. A., Bojičić, I., & Frew, D. J. 2017, in IAU Symp. 323, Planetary Nebulae: Multi-Wavelength Probes of Stellar and Galactic Evolution, ed. X. Liu, L. Stanghellini, & A. Karakas (Cambridge: Cambridge Univ. Press), 36
Peimbert, A., Peimbert, M., Delgado-Inglada, G., García-Rojas, J., & Peña, M. 2014, RMxAA, 50, 329
Peimbert, M., Luridiana, V., & Torres-Peimbert, S. 1995, RMxAA, 31, 147
Phillips, J. P., & Márquez-Lugo, R. A. 2011, RMxAA, 47, 83
Ramos-Larios, G., Phillips, J. P., Richer, M. G., & Kemp, S. N. 2008, MNRAS, 387, 415
Redman, M. P., Viti, S., Cau, P., & Williams, D. A. 2003, MNRAS, 345, 1291
Sahai, R., Morris, M. R., & Villar, G. G. 2011, AJ, 141, 134
Saitō, M., Iwata, I., Okumura, S.-i., Mori, A., & Yamashita, T. 1999, PASJ, 51, 673
Schmidt, D. R., Woolf, N. J., Zega, T. J., & Ziurys, L. M. 2018b, Natur, 564, 378
Schmidt, D. R., Zack, L. N., & Ziurys, L. M. 2018a, ApJL, 864, L31
Schmidt, D. R., & Ziurys, L. M. 2016, ApJ, 817, 175
Schmidt, D. R., & Ziurys, L. M. 2017a, ApJ, 835, 79
Schmidt, D. R., & Ziurys, L. M. 2017b, ApJ, 850, 123
Schmidt, D. R., & Ziurys, L. M. 2019, ApJL, 881, L38
Schwarz, H. E., Corradi, R. L. M., & Melnick, J. 1992, A&AS, 96, 23
Snow, T. P., & McCall, B. J. 2006, ARA&A, 44, 367
Stanghellini, L., Corradi, R. L. M., & Schwarz, H. E. 1993, A&A, 279, 521
Stanghellini, L., Shaw, R. A., & Villaver, E. 2008, ApJ, 689, 194
Stasińska, G., Górny, S. K., & Tylenda, R. 1997, A&A, 327, 736
Sterling, N. C., & Dinerstein, H. L. 2008, ApJS, 174, 158
Tenenbaum, E. D., Dodd, J. L., Milam, S. N., Woolf, N. J., & Ziurys, L. M. 2010, ApJS, 190, 348
Tenenbaum, E. D., Milam, S. N., Woolf, N. J., & Ziurys, L. M. 2009, ApJ, 704, L108
Tylenda, R., Siódmiak, N., Górny, S. K., Corradi, R. L. M., & Schwarz, H. E. 2003, A&A, 405, 627
van der Tak, F. F. S., Black, J. H., Schöier, F. L., Jansen, D. J., & van Dishoeck, E. F. 2007, A&A, 468, 627
van Hoof, P. A. M., van de Steene, G. C., Beintema, D. A., et al. 2000, ApJ, 532, 384
Weidmann, W. A., & Gamen, R. 2011, A&A, 526, A6
Woods, P. M., Nyman, L.-Å., Schöier, F. L., et al. 2005, A&A, 429, 977
Zack, L. N., & Ziurys, L. M. 2013, ApJ, 765, 112
Zeigler, N. R., Zack, L. N., Woolf, N. J., & Ziurys, L. M. 2013, ApJ, 778, 16
Zhang, C. Y., & Kwok, S. 1990, A&A, 237, 479
Zhang, C. Y., & Kwok, S. 1993, ApJS, 88, 137
Zhang, Y., Kwok, S., & Dinh-V-Trung 2008, ApJ, 678, 328
Zijlstra, A. A., Pottasch, S. R., & Bignell, C. 1989, A&AS, 79, 329
Ziurys, L. M. 2019, in The Handbook of Astrobiology, ed. V. Kolb (Boca Raton: CRC Press), 147
Ziurys, L. M., Schmidt, D. R., & Woolf, N. J. 2020, ApJL, 900, L31